The effect of Ag, Pb and Bi impurities on grain boundary sliding and intergranular decohesion in Copper

Georg Schusteritsch,[1,*] Thomas D. Kühne,[2,3] Zheng Xiao Guo,[4,5] and Efthimios Kaxiras[1,6]

[1] *School of Engineering and Applied Sciences, Harvard University, Cambridge, MA 02138, USA*

[2] *Institute of Physical Chemistry and Center for Computational Sciences, Johannes Gutenberg University of Mainz, D-55128 Mainz, Germany*

[3] *Department of Chemistry, University of Paderborn, D-33098 Paderborn, Germany*

[4] *Department of Chemistry, University College London, London WC1H 0AH, United Kingdom*

[5] *London Centre for the Theory and Simulation of Materials, London WC1E 6BT, United Kingdom*

[6] *Department of Physics, Harvard University, Cambridge, MA 02138, USA*

(Dated: June 30, 2016)

Abstract

We investigate the changes in grain boundary sliding (GBS) and intergranular decohesion in copper (Cu), due to the inclusion of bismuth (Bi), lead (Pb) and silver (Ag) substitutional impurity atoms at a $\Sigma5\,(012)$ symmetric tilt grain boundary (GB), using a first-principles concurrent multiscale approach. We first study the segregation behavior of the impurities by determining the impurity segregation energy in the vicinity of the GB. We find that the energetically preferred sites are on the GB plane. We investigate the intergranular decohesion of Cu by Bi and Pb impurities and compare this to the effect of Ag impurities by considering the work of separation, W_s and the tensile strength, σ_t. Both W_s and σ_t decrease in the presence of Bi and Pb impurities, indicating their great propensity for intergranular embrittlement, whilst the presence of Ag impurities has only a small effect. We consider GBS to assess the mechanical properties in nanocrystalline metals and find that all three impurities strongly inhibit GBS, with Ag having the biggest effect. This suggests that Ag has a strong effect on the mechanical properties of nanocrystalline Cu, even though its effect on the intergranular decohesion properties of coarse-grained Cu is not significant.

PACS numbers:

61.72.Mm Grain and twin boundaries

62.20.M- Structural failure of materials

71.15.Mb Density functional theory, local density approximation, gradient and other corrections

62.25.-g Mechanical properties of nanoscale systems

68.35.Dv Composition, segregation; defects and impurities

Keywords: grain boundaries, grain boundary sliding, intergranular decohesion, density functional theory

*Present address: Department of Materials Science and Metallurgy, University of Cambridge, 27 Charles Babbage Road, Cambridge CB3 0FS, United Kingdom; Electronic address: gs550@cam.ac.uk

I. INTRODUCTION

Grain boundary sliding (GBS) and intergranular decohesion are important processes which determine the mechanical properties of metals. Intergranular decohesion is connected to the brittle behavior of polycrystalline materials and has been studied primarily in the context of coarse-grained metals [1–4]. To assess the mechanical properties of coarse-grained metals, intergranular decohesion is often taken as a competing effect to dislocation nucleation [3–5]. GBS has long been known [6–8] to be important for the plastic flow in polycrystalline materials at high temperatures ($T > 0.4\ T_m$, where T_m is the melting temperature). GBS is also thought to play a major role in experiments of nanocrystalline Cu where superplasticity has been demonstrated at low temperatures [9]. The importance of GBS as a deformation mechanism in pure nanocrystalline metals has been studied computationally using classical molecular dynamics (MD) [10–18]. A cross-over for decreasing grain size from a regime where plasticity is dominated by dislocation mediated activity to a regime where GBS is the dominant process was observed [10–16]. Schiøtz and co-workers [14–16] proposed that GBS, as an alternative deformation mechanism, can explain the apparent break-down of the Hall-Petch relation observed in nanocrystalline metals [19, 20]. It is still unclear to what extent and at which grain sizes GB-mediated processes dominate dislocation-mediated processes [13, 17, 18, 21]. Recent experiments have for instance shown evidence of GBS for grain sizes as large as 135 nm [22], whilst further MD studies showed that dislocation activity may still play an important role even at nanoscale-sized grains [17, 18]. The latter findings nevertheless at the same time show evidence for the great importance of GBS as a deformation mechanism in nanocrystalline metals, even if dislocation-mediated processes occur simultaneously. A deeper understanding of the underlying processes of both GBS and intergranular decohesion is important in the development of modern metallic structures, in particular for those that involve nanocrystalline features.

The mechanical properties of metals can change dramatically when they are exposed to chemical impurities [6, 23, 24]. The GB segregation behavior of impurities and self-interstitials was studied computationally for α-Fe [25–28], Al [29], Ni [1] and Cu [30], employing a variety of approaches ranging from Lennard-Jones potentials to full first-principles treatment. Several studies have attempted to elucidate the correlation of these properties to the exact GB structure [26–28, 31]. The influence of impurities on intergranular decohesion

has been studied in the past primarily in the context of coarse-grained metals by considering the work of separation and tensile strength for Cu [2, 3]], Fe [26, 28], Al [29] and Ni [1, 5, 32] GB's with a variety of segregated impurities. To address ductile behavior in coarse-grained materials, either the unstable stacking energy in the context of dislocation nucleation is calculated using ab initio techniques [5] or dislocations were simulated directly using primarily classical MD studies [31]. Most theoretical studies on GBS in nanocrystalline metals have dealt only with pure systems or systems with vacancies [33–37]. Only a very limited number of studies have tried to address the issue of chemical impurities and how these may affect the physics of GBS in nanocrystalline metals. Most experimental results are in the context of GBS in high temperature superplasticity, rather than for the lower temperatures where GBS is expected for nanocrystalline metals. Experiments by Yin et al [38] suggest that sulfer interstitials hinder GBS in nanocrystalline Ni. Experiments on GBS are however exceedingly difficult: Conflicting findings on the effect of impurities on GBS in Al have for instance been reported [39–43]. Our understanding of the influence impurities have on the mechanical behavior of nanocrystalline metals at an atomistic level is still very limited, but computational studies can aid in unraveling this complex problem. Millet et al [30] have considered GB migration of a Cu GB using a Lennard-Jones potential and found the dopant size of impurities to be of crucial importance to suppress GB migration. The influence of sulfur impurities on a Nickel GB was studied in Ref. [5] and it was found that these inhibit GBS. Du et al [44] studied GBS in an Al bicrystal with segregated Mg and Si impurities and find that Mg strongly hinders GBS, with Si having the opposite effect. It was suggested this is a result of stronger bonding of Al with Mg than with Si. We will consider here copper as a prototypical ductile metal that exhibits significant changes in its mechanical behavior when chemical impurities are present. Impurities in coarse-grained Cu tend to segregate to the GBs and lead to chemical embrittlement [2, 3, 45, 46]. The nanocrystalline form of Cu has recently become a candidate for applications. To elucidate the role of impurities on the macroscopic mechanical behavior in both coarse-grained and nanocrystalline Cu, we study GBS and intergranular decohesion in Cu at a $\Sigma 5\,(012)$ GB and consider the influence of three impurities bismuth (Bi), lead (Pb) and silver (Ag). Separating the overall macroscopic behavior into processes that can be treated individually at the atomic level can lead to useful predictions of the behavior of materials and similarly allows us to understand the underlying physics and chemistry. Bi, Pb and Ag are common impurity elements in Cu

and are known to segregate to the GBs [47, 48]. Although the effect of impurities on Cu in the context of coarse-grained metals has been studied experimentally and theoretically in the past, little is known of their effects on GBS as a competing mechanism of intergranular decohesion in nanocrystalline Cu.

In this work we first establish the energetically preferred positions of the three different impurities near the GB. We find that the substitutional sites near the GB are energetically more stable than those in the bulk, with the lowest energy position being located on the GB plane. The influence of chemical impurities on the Cu GB is related to the work of separation, W_s, and the tensile strength, σ_t. These two quantities are directly linked to the cleavage properties of the metal-impurity system since they quantify the propensity of GBs to fail via intergranular fracture in the context of both crack nucleation and propagation [1–5, 49]. We show evidence of chemical embrittlement of Cu in the presence of Bi and Pb impurities, due to a significant decrease in both W_s and σ_t. In the presence of Ag impurities, the intergranular behavior changes little in comparison to the pure Cu GB. This is consistent with previous work that found that Ag does not affect significantly the behavior of coarse-grained Cu [3]. We then study the effect of impurities on GBS. We find that both Bi and Pb inhibit GBS, resulting in a decrease of ductile behavior. The effect of Ag is somewhat surprising: Although it does not alter the behavior of coarse-grained Cu, we predict that in nanocrystalline Cu the presence of Ag strongly inhibits GBS. This may be of great significance for experiments and future technological applications.

The paper is organized as follows: Section II briefly reviews our computational method, with the first-principles multiscale approach discussed in Appendix A. In Section III we present results for the impurity segregation energy near the GB, followed by our results on how Bi, Pb and Ag impurities influence intergranular decohesion of the $\Sigma5\,(012)$ Cu GB in Section IV. The results for GBS of the pure Cu GB and of the Cu GB with Bi, Pb, and Ag are presented in Section V. Finally, we present our conclusions in Section VI.

II. COMPUTATIONAL METHOD

We employ a multiscale approach for studying the GBS and intergranular decohesion processes in Cu. The method is based on coupling a small region containing the GB and the impurities, which is treated with density functional theory (DFT) [50], to the bulk,

which is treated by the embedded atom method (EAM) [51]. This concurrent multiscale approach allows us to achieve quantum mechanical accuracy near the GB and for the segregated defects. It can therefore account for bond breaking and bond forming processes in a chemically diverse environment which is difficult to capture by other computational methods. At the same time, the multiscale approach makes it possible to keep the computational cost at a minimum, so that large systems can be investigated. The multiscale method has been successfully used in the past [52–54] and our implementation is summarized for completeness in Appendix A. The quantum mechanical (QM) region is treated using DFT as implemented in the suite of programs cp2k [55, 56]. We use the generalized gradient approximation of PBE [57] to approximate the exchange-correlation energy and separable and norm-conserving GTH pseudopotentials to describe the interactions between the valence electrons and the ionic core [58, 59]. The quantum mechanical region of the multiscale method is described using a double-ζ (DZVP) basis for the calculations of intergranular decohesion. To further reduce computational cost a single-ζ basis, optimized in molecular calculations (m-SZV) to become approximately equivalent to a DZVP basis [60] was used for the GBS and impurity segregation results. Convergence of the PW grid required a density cutoff of 525 Ry and 320 Ry for the two sets of calculations, respectively. The classical region is treated using the embedded atom method with the EAM1 potential of Mishin *et al.* [61], rescaled to match the lattice constant and the bulk modulus of the QM region.

We considered here the $\Sigma5\,(012)$ symmetric tilt GB in Cu. The GB formation energy is 0.92 J/m^2, which compares well with previously reported values for the same type of GB in Cu ($0.878 - 1.27$ J/m^2 [37, 61]). As in most similar computational studies, we consider a single symmetric tilt GB, with the expectation that other GBs, that share structural similarities, will behave in a similar manner. The multiscale supercell consists of 3216 Cu atoms, with appropriate substitutions by impurity atoms in the GB region. The structure has 201 planes parallel to the GB plane, with 16 atoms per plane. All our structures are relaxed to account for GB expansion. Structural relaxations are performed using either the conjugate gradient [62] or limited-memory Broyden-Fletcher-Goldfarb-Shanno (L-BFGS) quasi-Newton method [63, 64].

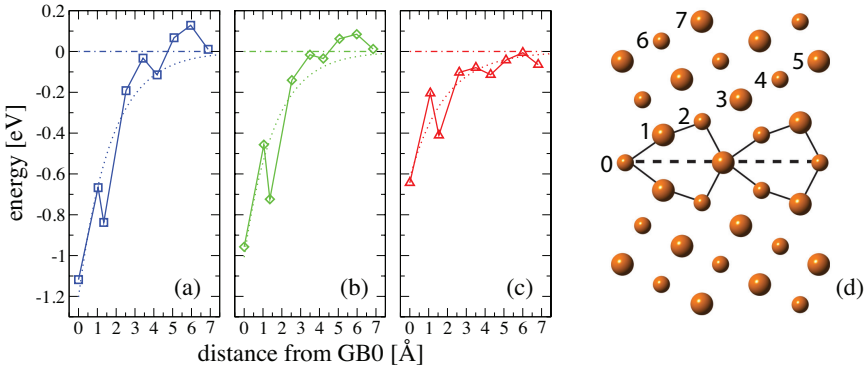

FIG. 1: Segregation energy as a function of distance to the GB for (a) Bi, (b) Pb and (c) Ag impurities. An exponential fit to illustrate the behavior of the impurity concentration near a GB is shown as a dotted line (solid lines connecting individual data points are guides to the eye). A small portion of the atomic structure of the Cu GB is shown in (d), with labels $0, 1, ...$ indicating the planes of Cu atoms parallel to the GB for which impurities are substituted to determine the segregation energy. The GB plane is located at label 0. One impurity is placed on a substitutional site on a plane with Cu atoms. Small and large circles are atoms in the adjacent {001} planes.

III. IMPURITY SEGREGATION ENERGY NEAR THE GRAIN BOUNDARY

Impurities in Cu are known to segregate to GBs under equilibrium [47, 48]. The formation energy for impurity X, ε_f^X, is defined in general as:

$$\varepsilon_f^X = \frac{1}{n_i}\left[E_{tot}^X(n_i, n_h) - E_{tot}\left(n_h^0\right) - n_i\mu_i - \left(n_h - n_h^0\right)\varepsilon_h\right], \tag{1}$$

where $E_{tot}\left(n_h^0\right)$ is the energy of the system with no impurities and n_h^0 host atoms, $E_{tot}^X(n_i, n_h)$ is the energy of the system with n_i impurities of type X, and n_h host atoms, ε_h is the energy per atom of the metal matrix host in its ideal structure and μ_i is the chemical potential of the impurities. We consider here the segregation energy E_{seg} defined as the energy difference between the formation energy of an impurity near the GB and the formation energy of an impurity in the bulk, $E_{\text{seg}} = \varepsilon_f^X\,(GB) - \varepsilon_f^X\,(fcc)$. For a single substitutional impurity, $n_i = 1$, this simplifies to,

$$E_{\text{seg}} = \left[E_{tot}^X(\text{GB}) - E_{tot}\,(\text{GB})\right] - \left[E_{tot}^X\,(\text{fcc}) - E_{tot}\,(\text{fcc})\right]. \tag{2}$$

	segregation energy [eV]	
system	this work	expt./other theory
Ag	-0.64	$-0.41^{(a)}$
Pb	-0.96	-1.40 to $-1.47^{(b)}$
Bi	-1.12	$-0.94 \pm 0.11^{(c)}$, -1.32 to $-1.58^{(b)}$

TABLE I: Segregation energy for Bi, Pb and Ag impurities at their lowest energy positions (see Fig. 1). For comparison experimental and other computational results are shown for similar GB systems. $^{(a)}$: experiments Ref. 73, $^{(b)}$: theory Ref. 2 and $^{(c)}$: experiments Ref. 74.

The structures for the calculations of the segregation energy are based on a Cu GB with all atomic positions relaxed and care was taken to fully relax the bulk strain. We place a single substitutional impurity at different lattice sites, with all atomic positions fully relaxed after the impurities are added. The segregation energy is shown as individual data points in Fig. 1 (a), (b) and (c) for Bi, Pb and Ag, respectively for the different positions of the impurity atoms. The segregation energies of the energetically most stable positions for each impurity are compared to experimental and other computational results in Table I. The segregation energies near the GB are lower than the bulk value for all three impurities, with the lowest energy position for all three impurities located at the GB plane. Impurities situated one layer from the GB plane have energy higher than those situated two layers away from the GB plane. The energy approaches that of the bulk value at around four to eight layers away from the GB plane. The variation of the segregation energy for layers four to eight planes away from the GB is not surprising, as the GB produces a perturbation that can still be felt at a large distance from its center. We also provide an exponential fit to the calculated energy values (shown as a dotted line) to illustrate the expected behavior of the impurity segregation. The greatest segregation energy was found for Bi, closely followed by Pb. The segregation energy of Ag is almost half that of Bi.

IV. INTERGRANULAR DECOHESION

To address the issue of intergranular decohesion we study the effect that Bi, Pb and Ag impurities have on the $\Sigma 5\,(012)$ Cu GB. The Bi-Cu system has been studied extensively, and

several studies have found a segregation concentration of around 1 monolayer (ML) to be consistent with chemical embrittlement [47, 65]. Scanning transmission electron microscopy studies have identified the preferred locations of the Bi impurities for the $\Sigma5$ GB to be at the GB plane [45], consistent with our results in Section III. We therefore place the Bi impurities as substitutional defects with 1 ML coverage on the GB plane, as in previous theoretical work with similar GB structures [2, 3, 46]. This corresponds to an impurity areal density of approximately 0.066 Å^{-2}. To allow for consistent comparisons, the same concentration and positions are chosen for the Ag and Pb impurities. This choice is appropriate considering recent experiments on nanocrystalline Cu in which up to 1.1 ML coverage was found for the segregation of Ag to GBs [66].

The supercell contains 11 layers of DFT atoms, corresponding to a quantum region of size 16.41 Å ×14.68 Å ×8.48 Å. Convergence tests of up to 27 layers (16.41 Å ×14.68 Å ×21.65 Å) showed that the results change by less than 5%. As impurities are added to the GB plane the GB structure changes. We consider the distance between 30 layers on either side of the GB plane, and define the GB expansion, d_{GB}, as the change of this length as we add impurities. We list the respective values of the GB expansion in Table II. The GB expansion, d_{GB}, is particularly large for Bi and Pb with an increase of the GB region by 0.82 Å and 0.94 Å, respectively. The GB expansion corresponding to the case of Ag impurities is much smaller, hinting at the smaller propensity of Ag to cause chemical embrittlement for the $\Sigma5\,(012)$ GB. This behavior is qualitatively similar to the GB expansion for a $\Sigma5\,(013)$ Cu GB reported by Lozovoi *et al.* [3]. For comparison, the substitution of one Cu atom in a 500 atom cell of fcc Cu by one impurity atom results in a lattice vector increase of 0.007, 0.014 and 0.016 Å for Ag, Pb and Bi, respectively, showing a similar trend for each atomic type.

The difference in the structural changes for the different impurities can be further quantified by considering the energetics of cleavage. We simulate cleavage by separating the GB at the center and rigidly displacing the two grains by a given distance, δ. The cell size perpendicular to the GB plane is appropriately relaxed. Interlayer relaxations are dominant, whilst in-plane relaxations of the cleavage plane atoms are negligible and are hence not included in calculations for the decohesion energy as a function of grain separation, δ. In Fig. 2 (a) we show the decohesion energy as a function of δ for four systems, the pure Cu GB, and the Cu GB with Ag, Bi and Pb impurities. This set of results shows different behavior for the Bi and Pb impurities in comparison to the pure Cu GB or the Cu GB with Ag impurities.

system	d_{GB} [Å]	W_{s} [J/m^2]	σ_t [GPa]	$\gamma^{(\mathrm{b})}$ [J/m^2]	$\gamma^{(\mathrm{b})} - \gamma^{(\mathrm{c})}$ [J/m^2]	$D = W_{\mathrm{s}}/\gamma^{(\mathrm{b})}$
pure	-	2.65	16.2	0.18	0.18	14.2
Ag	0.26	2.47	15.5	0.70	0.23	3.5
Pb	0.82	1.54	9.1	0.49	0.15	3.2
Bi	0.94	1.38	7.7	0.31	0.06	4.4

TABLE II: Work of separation, W_s, tensile strength, σ_t, GB expansion, d_{GB}, GBS energy, γ, and ductility parameter, D, for the clean Cu $\Sigma5\,(012)$ GB and with substitutional Ag, Pb and Bi impurities at the GB plane with a coverage of 1 ML or an impurity concentration of 0.066Å^{-2}.

To quantify the potential of the different systems to fail in an intergranular fashion, we first consider the work of separation, W_s, defined as,

$$W_s = E_\infty - E_0, \tag{3}$$

where E_∞ and E_0 are the total energies of the separated grains and the intact GB, respectively. Pb and Bi induce a significant decrease of the work of separation in comparison to the pure Cu GB, by 1.11 J/m^2 and 1.27 J/m^2 or 42% and 48%, respectively. For Ag this decrease is only 0.18 J/m^2 or 7%. Since the work of separation is directly related to how easily a crack can spread along the GB interface [4], we conclude that intergranular embrittlement is greatly enhanced by the segregated Bi and Pb impurities, whereas Ag impurities have a negligible effect. The energy release rate for dislocation nucleation, G_{disl} [4, 49] for a typical coarse-grained Cu GB system lies in the range of $1-2$ J/m^2 [67]. Thus, the pure GB and that with Ag impurities has $G_{\mathrm{cleave}} = W_s > G_{\mathrm{disl}}$, whereas the addition of Bi or Pb impurities causes G_{cleave} to decrease leading to embrittlement of coarse-grained Cu.

As a second measure of intergranular fracture we consider the tensile strength, σ_t, as a function of impurity addition at the GB plane. This allows us to determine how easily a crack can nucleate at stress concentrations in the otherwise ductile Cu [4]. We calculate the stress, $\sigma\,(\delta)$, based on the decohesion energy curves of Fig 2(a) as the derivative with respect to the separation of the two grains. This is shown in Fig 2(b) with the tensile strength listed in Table II. The tensile strength decreases by a very small amount, 4.3%, when Ag impurities are added, but Pb and Bi impurities reduce σ_t by 44% and 52%, respectively. Appropriately accounting for relaxations was found to be important in describing the behavior of the

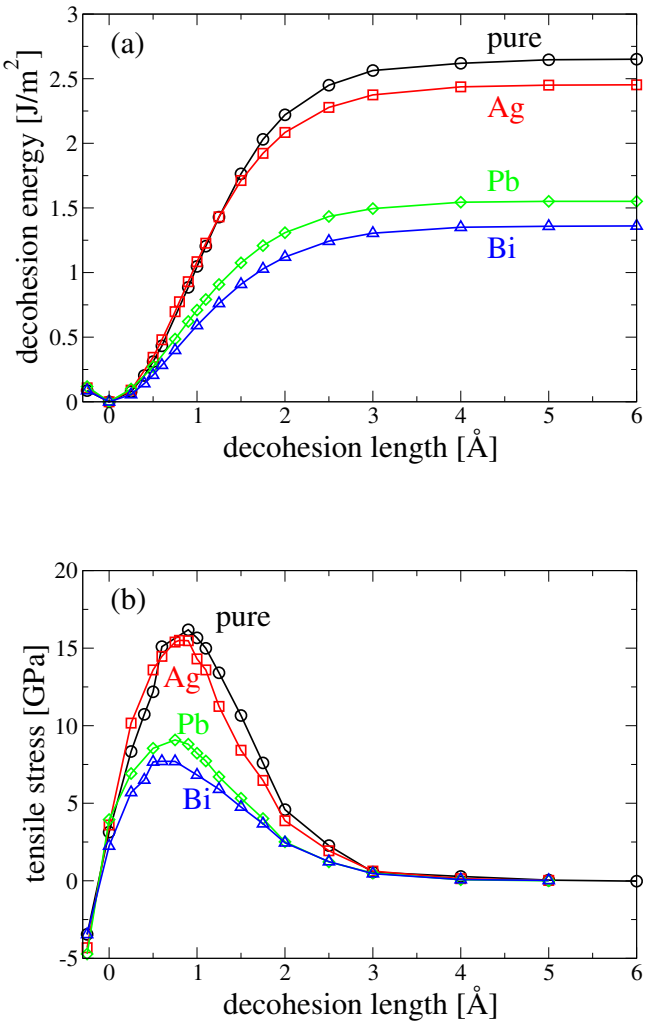

FIG. 2: (a) Decohesion energy as a function of the decohesion length for the pure Cu $\Sigma5\,(012)$ GB (black circles), the Cu GB with Ag (red squares), Pb (green diamonds) and Bi (blue triangles) impurities. (b) Stress as a function of decohesion length for the pure Cu GB, the Cu GB with Ag, Pb and Bi impurities. Solid lines are guides to the eye.

Cu GB system. As a comparison, ideal brittle cleavage, often employed as a first-order approximation in calculating the tensile strength due to its significantly lower computational cost [1], yielded results up to 20% different.

To elucidate the origin of these effects that the impurities produce, we examine the changes in the electronic structure of the material near the grain boundary induced by the presence of the impurities. To this end, we show in the top row of Fig. 3 the electronic

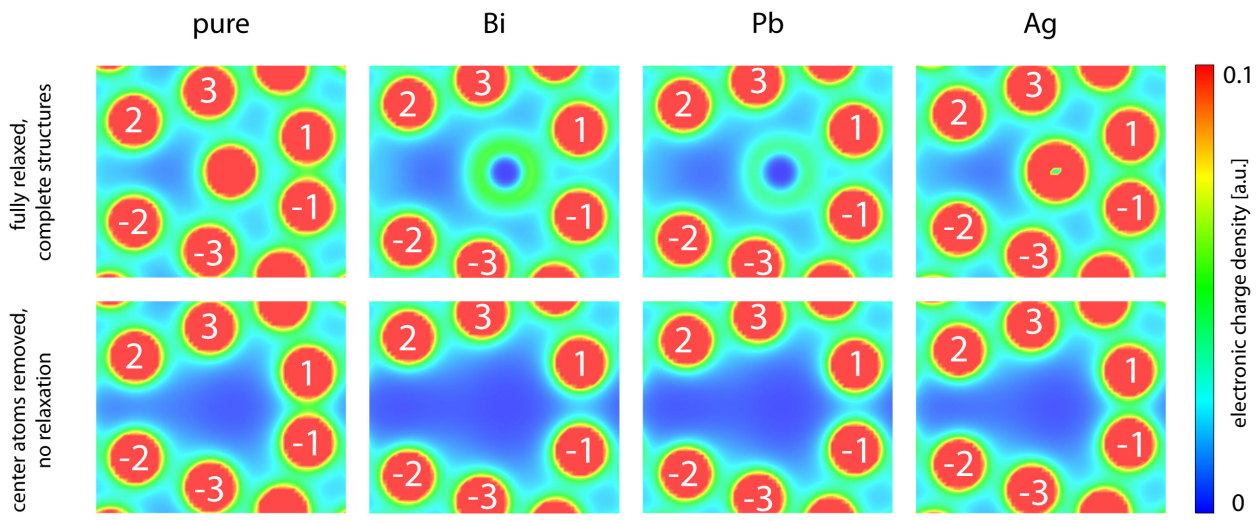

FIG. 3: Electronic charge density on the (001) plane intersecting the GB. The top row shows fully relaxed structures of the pure $\Sigma5\,(012)$ Cu GB, and the $\Sigma5\,(012)$ Cu GB with substitutional Bi, Pb and Ag impurities. The bottom row shows the charge densities of the same structures as in the row above, but with the Cu or impurity atoms at the GB plane removed (no further relaxations are allowed). Atoms in the first three sets of symmetric planes away from the GB plane are labeled $-3, \ldots, 3$. Red areas are regions of high electronic charge density, blue areas are regions of low electronic charge density.

charge density for the pure Cu GB and the Cu GBs with Bi, Pb and Ag impurities. The bottom row of this figure shows the charge density of the same structures, with no further relaxations, but with all Cu or impurity atoms at the GB plane removed. For each case, the charge density is shown for the (001) plane which perpendicularly intersects the GB plane. For the pure GB the strongest bond across the GB interface, in terms of charge density, is the Cu-Cu bond between the two layers just adjacent to the GB plane (labeled as 1 and -1 in Fig. 3). When Bi and Pb impurities are added to the GB, this Cu-Cu bond shows a significant depletion of electronic charge. This change in electronic charge distribution is a result of the structural changes induced by the substitutional Bi and Pb impurities, as is evident from the comparison of the charge densities of the top row to the bottom row in Fig. 3. The electronic charge density between Cu atoms in the 1 and -1 planes, that play a crucial role in bonding across the GB interface and hence its cohesion, remains approximately unchanged when the atoms on the GB plane are removed. This means that adding or removing Bi and Pb atoms does not significantly affect the electronic charge

density of the Cu-Cu bond across the GB interface. It is instead the actual GB *expansion* caused by adding the impurity atoms that causes the depletion of charge. In other words, our results suggest that the dominant changes in the electronic charge density are due to a structural effect and not due to the chemical character of the Bi or Pb impurities. One can even see that the electronic charge density between the Cu atoms *increases* as Bi atoms are added, albeit this is not a strong effect. The electronic charge density for the structures with Ag impurities are also shown in Fig. 3. There is no significant difference to the electronic charge density of the pure Cu GB, which is consistent with its very small propensity to cause intergranular embrittlement.

This analysis is in agreement with earlier work by Lozovoi *et al* [3] who studied a $\Sigma5\,(013)$ Cu GB and the effect Bi and Ag have on the intergranular decohesion. They analyzed the effect in terms of three different contributions, the host-removal (HR), the substitutional-structure (SS) and the chemical and compressed impurity (CC) processes in order to elucidate the importance of electronic effects compared to purely structural effects. These three processes quantify the energy cost of (i) removing a metal matrix atom, (ii) the purely structural changes associated with adding a substitutional impurity to the metal matrix, and (iii) the chemistry of the impurity atoms in combination with the compression they feel, respectively. The definition of each term had originally been introduced in Ref. [3], but is reviewed for completeness in Appendix B. For the $\Sigma5\,(013)$ GB, they reported a strong negative contribution of the substitutional structure term of $SS = -0.39$ J/m^2 (-1.25 J/m^2) for Bi and $SS = -0.04$ J/m^2 (-0.37 J/m^2) for Ag with 0.5 ML (1.0 ML) coverage, corresponding to 0.0508Å^{-2} (0.1016Å^{-2}) impurity areal density. The results for the $\Sigma5\,(012)$ GB studied here are similar, where the substitutional structure process contributes SS $= -0.53$ J/m^2 for Bi and SS $= -0.08$ J/m^2 for Ag with 1 ML coverage, corresponding to 0.066Å^{-2} impurity areal density. For the same impurity concentration as above, the chemical and compressed impurity terms for the $\Sigma5\,(013)$ GB were reported to be $CC = 0.34$ J/m^2 (0.83 J/m^2) for Bi and $CC = 1.20$ J/m^2 (1.83 J/m^2) for Ag. In comparison for 1 ML we find $CC = 0.83$ J/m^2 for Bi and $CC = 1.49$ J/m^2 for Ag. Any quantitative differences for the substitutional structure processes can likely be traced back to the structural differences of the two GBs. The $\Sigma5\,(012)$ GB has perfectly symmetric substitutional positions at the GB plane, whereas the $\Sigma5\,(013)$ GB has two geometrically different positions, of which one has a tighter spatial confinement. This likely results in a greater substitutional structure term, since, for

the same impurity coverage, the $\Sigma5\,(013)$ GB must be deformed much more significantly than the $\Sigma5\,(012)$ GB. The smaller substitutional changes result in a smaller propensity to cause embrittlement for the $\Sigma5\,(012)$ Cu GB. For the same Bi impurity coverage, that is, 1 ML coverage, the work of separation of the $\Sigma5\,(012)$ GB is reduced by 48%, whereas the $\Sigma5\,(013)$ GB experiences a 71% decrease of the work of separation for 1 ML and 36% for 0.5 ML coverage [3]. This underscores the importance of mechanical distortions in the intergranular embrittlement of Cu GBs. By considering the impurity areal density to normalize the results, there is good agreement of the behavior for the two different GBs, suggesting that the trends and conclusions outlined above are general to these types of GBs.

V. GRAIN BOUNDARY SLIDING

A. Pure system

We first discuss GBS for the pure $\Sigma5\,(012)$ Cu GB. To model this process, we slide the two half crystals on either side of the GB against each other along $\langle 012\rangle$, which is a vector of the coincidence site lattice (CSL) of the $\Sigma5\,(012)$ coherent tilt GB. Our calculations are based on simulating sliding quasistatically, that is, the two grains are shifted rigidly against each other. After sliding, all slip plane atoms are held fixed in the in-plane directions but are allowed to relax freely in the direction perpendicular to the GB plane. This is to ensure that the slip plane vectors can be appropriately defined [5]. All other atoms are allowed to fully relax. The 27 planes surrounding the GB are treated by DFT. The energy for GBS of the pure system is shown in Fig. 4. Extrema occurr at slip displacements of approximately $s = 0.0$, 0.2, 0.4, 0.7 and 1.0 in units of the full periodic displacement along $\langle 012\rangle$. These are labeled as (a),(b),(c),(d) and (e) in Fig. 4, respectively. Important GBS energies labeled as $\gamma^{(x)}$ are listed in Table II, where $x = \mathrm{a}, ..., \mathrm{e}$. The atomic positions of these slip displacements are shown in Fig. 5, where atoms on parallel $\{001\}$ planes are indicated with larger and smaller circles. The GB plane is indicated as a dashed black line, and remains centered on the same atoms. The first of these structures, labeled (a), is the lowest energy GB structure with no slip displacement. We have included characteristic diamond shapes across the GB plane, showing the GB in the traditional way. The configuration corresponding to (e) is the structurally equivalent periodic displacement of (a). At (b), corresponding to $s = 0.2$, there

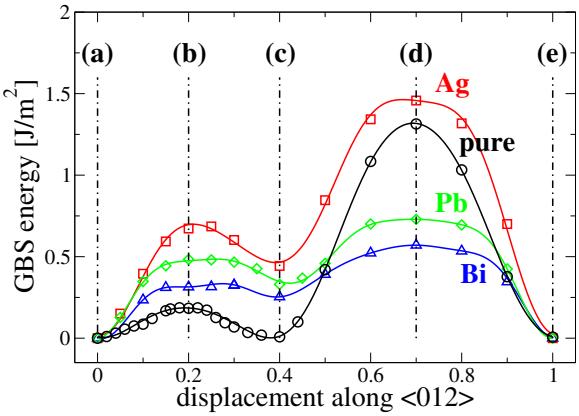

FIG. 4: GBS energy along the slip vector $\langle 012 \rangle$ for the $\Sigma 5\,(012)$ GB without impurities (black circles), and with Bi (blue triangles), Pb (green diamonds) and Ag (red squares) substitutional impurities. Solid lines are Fourier series fits. The dash-dotted vertical lines labeled (a) through (e) identify special configurations corresponding to energy extrema. The corresponding atomic structures are shown in Fig. 5.

is a local maximum in the energy, corresponding to the run-on configuration which places slip plane atoms of adjacent $\{001\}$ planes at the same coordinate along $\langle 012 \rangle$, resulting in a high-energy structure. The maximum of the energy is located at $s = 0.7$, corresponding to configuration labeled (d), and is also caused by a run-on configuration across the slip plane. In this case, slip plane atoms in the same (001) planes share the same in-plane coordinates, producing the global maximum of this energy for slip in this direction and a significant expansion around the GB plane. Due to symmetry, for a given applied shear stress the two half-crystals can slide so that GBS occurs along the lower energy run-on configuration (b) on the opposite side of the GB plane; this avoids the high-energy path passing through configuration (d).

Fig. 4 also shows a minimum at $s = 0.4$. This is a geometrically equivalent structure to the initial GB at $s = 0.0$, and the GB plane migrates one layer as a sliding event from (a) to (c) takes place. This is indicated by the dashed line, which lies on the atoms of the original GB plane, and the diamond shapes that indicate the new position of the GB plane. This coupled process of GBS and GB migration is similar to the findings by Lu *et al* [33] in their study of GBS in aluminum in the presence of vacancies.

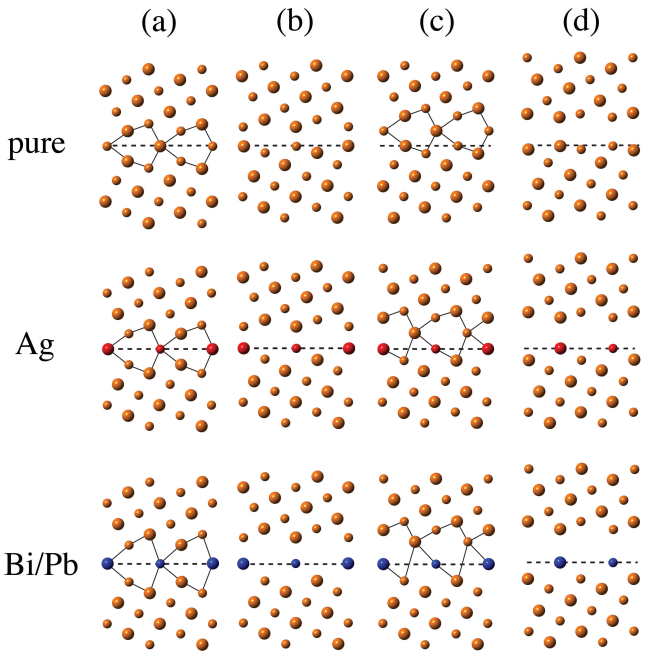

FIG. 5: Atomic structure for the slip displacements (a) $s = 0.0$, (b) $s = 0.2$, (c) $s = 0.4$, (d) $s = 0.7$ in units of the periodic slip displacement along $\langle 012 \rangle$. Orange, blue and red circles represent Cu, Bi and Ag atoms, respectively. The atomic structure for the pure GB (all Cu atoms) and that with Ag impurities are shown separately, whilst, to the eye, the configuration for the GB with Pb impurities is essentially identical to the one with Bi atoms (shown as type Bi/Pb). Small and large circles are atoms in the adjacent $\{001\}$ planes. The plane of the initial GB plane is indicated by a dashed black line for all displacements.

B. Impurity system

We next consider GBS in the presence of impurities at the GB plane. We again choose the positions for the lowest segregation energy found in Section III for all impurities and a concentration of 1 ML. We first discuss Bi and Pb, shown as blue triangles and green diamonds in Fig. 4, respectively. Both show a similar change in behavior. The maximum for $s = 0.20$ increases by a factor of 1.7 and 2.6 for Bi and Pb, respectively. This local maximum becomes energetically less preferred as a pathway for GBS; this means that GBS along this direction is inhibited by the inclusion of Bi and Pb impurities. Whilst position (c) was geometrically equivalent to position (a) for the clean GB, this is not the case for the

impurity systems. Instead, since the GB plane migrates by one (012) plane, the impurities are now one layer away from the GB plane. This can be seen for Bi and Pb in Fig. 5 (c), and helps to explain why the GBS energy has a local minimum at position (c) larger than the minimum at no slip displacement at position (a). The second maximum, for direct run-on configurations at point (d), exhibits a marked decrease in comparison to a clean GB. This decrease still leaves a larger barrier than the path through position (b) and hence would not be a preferred pathway for slip behavior. In quantifying the effect of impurities on GBS, we focus our attention here on the pathway of sliding from (a) to (b). That is we consider that impurities are initially at their lowest energy positions and assess how these impurities affect the energy cost required to perform a single slip event, that is their effect on the resistance of the GB against sliding from position (a) to (b). As in similar studies [5, 33, 36], we therefore do not have to explicitly consider any competition of diffusion and the coupled GB motion.

The inhibition of GBS in the presence of Bi and Pb impurities suggests a decrease in ductile behavior for nanocrystalline metals with Bi and Pb impurity addition, since inhibiting GBS suppresses plastic deformation. This decrease in ductile behavior is further amplified by considering the combined effect of GBS and intergranular decohesion. The ratio of W_s and $\gamma^{(b)}$, often referred to as the ductility parameter D [49, 68–71], is a useful measure for quantifying the combined effect. The values of the ductility parameter decrease significantly for both Bi and Pb impurities (see Table II), dropping well below the value for the pure system; we therefore expect a change from more ductile to more brittle behavior as Bi and Pb impurities are added to nanocrystalline Cu.

We next consider the effect of Ag impurities on GBS. The work of separation and the tensile strength of the pure Cu GB decrease by only a very small amount in the presence of Ag impurities, in contrast to the case of the Bi and Pb impurities. The GBS energy curve for Ag, shown in Fig. 4, however indicates that the changes to the sliding behavior are even more significant than for Bi and Pb. The energy of configuration (b), $\gamma^{(b)}$, increases by a factor of almost 4 in comparison to the clean GB. This means that GBS becomes energetically very unfavorable. The GBS energy of configurations (c) and (d) also increases in comparison to the clean GB. As in the case of the Bi and Pb impurity systems, the increase in the energy for configuration (c) is due to the impurities migrating with the GB to one layer away from the GB plane, which has higher energy (Fig. 1 (c)). For configurations where the sliding energy has a minimum, the structural changes when Ag is present in comparison

to the clean GB are not as significant as for Bi or Pb impurities (configurations (a) and (c) in Fig. 5). This effect on the Cu matrix when Ag is added is however more significant for the crystal structure at the maximum of the sliding barrier (position (b)) and plays an important role in understanding the strong effect Ag has on GBS. To assess the origin of the very different behavior of Ag in comparison to Pb and Bi impurities for GBS further, we adapt the method by Lozovoi *et al* [3] discussed briefly in Sec. IV and Appendix B. We can in the same way as for intergranular decohesion break the overall GBS process into three parts: host removal, substitutional structure and chemical and compressed impurity processes. Whilst for decohesion the substitutional effect on the Cu matrix structure was very small for Ag, it is now much more similar to that of Bi or Pb at the maximum sliding barrier (position (b)): $SS = 0.61$ J/m^2 for Ag, $SS = 0.72$ J/m^2 for Pb and $SS = 0.71$ J/m^2 for Bi. Much in the same way as for decohesion, the chemical and compressed impurity term, quantifying the chemical interactions involved with adding impurities, is larger for Ag than for Bi and Pb: $CC = 0.41$ J/m^2 for Ag, $CC = 0.12$ J/m^2 for Pb and $CC = -0.04$ J/m^2 for Bi. This strongly indicates that Ag, in contrast to its behavior for the decohesion process, now has a stronger substitutional effect on the Cu matrix during a sliding event, which in combination with the already strong chemical interaction term leads to the significant increase in the GBS barrier height. This seems consistent with the results of Du et al [44], who find GBS inhibited in Al with segregated Mg in contrast to Si that enhances GBS, which was explained by stronger bonding for the Al+Mg system. The results by Lozovoi et al [3] have previously shown that the atomic radius of impurities can not necessarily be used to predict the behavior for intergranular decohesion in Cu. Similarly, given that both Ag (160 pm) and Bi (160 pm) have very similar atomic radii but different behavior and Pb (180 pm) lies in between the other two in terms of its effect, yet has a larger atomic radius, we do not find the atomic radius to be a good descriptor to predict the behavior during grain boundary sliding in Cu (135 pm) [72].

Ag is traditionally considered to have little effect on the mechanical properties of Cu but the ductility parameter D is reduced to similar values as those found for Bi and Pb impurities (see Table II). Based on this, we predict that for nanocrystalline Cu, Ag may have a strong effect, since it removes GBS as a plastic deformation mechanism. The unique behavior of Ag may be important for two reasons. First, its strong effect on GBS and the insignificant effect on intergranular decohesion may allow for an experimental route to confirm the observation

of GBS in MD simulations on nanocrystalline Cu, especially since it is difficult to otherwise observe the GBS process directly in experiments. Second, since Ag does not significantly affect intergranular decohesion, it may provide a means to increase the hardness of Cu in the context of the Hall-Petch behavior for nanograined Cu, which is believed to be limited by GBS for small grains [14–16]. As in similar *ab initio* studies, we assess here trends for only a specific set of mechanisms that are known to be of importance for the mechanical behavior of nanocrystalline metals. We do not attempt to address the relative importance of GB mediated *versus* dislocation mediated processes in nanocrystalline metals.

VI. CONCLUSION

We have studied the $\Sigma5\,(012)$ GB in Cu and addressed the changes this GB experiences as different impurities are added. We consider intergranular decohesion as a mechanism for inducing brittle behavior, and GBS as a plastic deformation mechanism for nanocrystalline structures. We employed a multiscale method based on coupling a large EAM region to a small DFT region to enable quantum mechanical treatment of the GB region and proper treatment of the elastic behavior of the bulk away from the GB. We investigated the lowest energy positions of the impurities and established that the energetically preferred sites for Bi, Pb and Ag are at the center of the GB. The segregation energy approximately follows the exponential decay behavior expected for impurity segregation near GBs. We find that the GB expansion observed for Bi and Pb impurities is significantly greater than that for Ag impurities. This is further quantified by considering the work of separation, W_s, which decreases significantly for both Bi and Pb, but not for Ag impurities. As a result, the likelihood that an existing crack spreads along the interface increases when Bi and Pb are added to the GB. The work of separation $W_s = G_{\text{cleave}}$ for Ag impurities is greater than G_{disl}, the energy release rate for dislocation nucleation, whereas $G_{\text{cleave}} \approx G_{\text{disl}}$ when Pb and Bi impurities are added to the Cu GB. We also consider the stress as a function of grain separation, $\sigma\,(\delta)$, and the tensile strength, σ_t. Appropriately relaxing the system to account for the inherent ductility of the bulk Cu was found to be important, with an error in σ_t of up to 20% when relaxation is omitted. The tensile strength of the pure Cu GB and the Cu GB with Ag impurities are very similar in magnitude. In contrast the tensile strength for Pb and Bi decreases by 44% and 52%, respectively, relative to the pure case. This suggests

that cracks are more likely to nucleate at points of high stress concentration when Bi and Pb are present at the GB plane. We studied the electronic charge density of the various structures and found that it reveals weakening of Cu-Cu bonds across the GB interface. To assess the mechanical properties of nanocrystalline Cu we consider GBS and how it is affected by adding one ML of Bi, Pb or Ag impurities. We find that both Bi and Pb inhibit GBS. Ag is an even stronger GBS inhibitor than Bi or Pb, which, in contrast to intergranular decohesion, can be attributed to the more significant effect Ag has on the Cu matrix for GBS in combination with strong chemical interactions. We examined intergranular decohesion and GBS as competing mechanisms by considering the ductility parameter D. We find that both Bi and Pb are expected to strongly embrittle the Cu GB, which is consistent with experiments. For Ag we find an overall decrease in ductile behavior, primarily due to the elimination of GBS as a form of plastic behavior. This is very different from the behavior of Ag in coarse-grained Cu. In general, these findings highlight how different the impurity effects can be on the mechanical properties of metals at the nanoscale; they also suggest that generalizations based on findings for coarse-grained materials can potentially be misleading.

VII. ACKNOWLEDGEMENTS

This work was supported in part by the Department of Energy, SciDac Grant ER-25788, and a gift from Intel Corporation. TDK acknowledges financial support from the Graduate School of Excellence MAINZ and the IDEE project of the Carl Zeiss Foundation. We thank the Academic Computing Group of the School of Engineering and Applied Sciences and the FAS Research Computing Group for computational resources. We gratefully acknowledge discussions with Frans Spaepen.

Appendix A: Multiscale Method

We describe here the essential features of the multiscale method. As in earlier work [52–54], the present method is based on taking into account the different contributions to the total energy of the whole system, and its derivatives with respect to atomic positions which give the forces. This method was originally developed using Orbital-Free DFT (OF-DFT) [52]. Here, we use KS-DFT, where the kinetic energy is known exactly in terms of

single-particle orbitals, which offers several advantages over OF-DFT: First and foremost, it allows treatment of transition metals like Cu (the focus of the present study) whereas OF-DFT is often limited to main group metals [75, 76]. There have been attempts to create appropriate local pseudopotentials and special kinetic energy density functionals for transition metals recently, but these are still limited in their applicability and transferability. It is also not clear how well these OF-DFT methods would perform for impurity inclusion as they are found to be of limited accuracy for alloy systems [77]. An additional complication is that the multiscale approach is best implemented with a method allowing for non-periodic boundary conditions. Although there are non-periodic approaches to OF-DFT [78], this is not trivial. In contrast, numerous choices exist for accurate treatment of non-periodic boundary conditions within KS-DFT [79–81]. We implement the multiscale method in the framework of a well-established KS-DFT code, which offers the advantages of versatility and transferability beyond the specific systems studied in the present work.

The supercell of the multiscale method is divided into two regions, I and II, treated by the quantum mechanical (KS-DFT) and classical (EAM) approaches, respectively. The total energy is given by

$$E\left[\mathrm{I}+\mathrm{II}\right] = E_1\left[\mathrm{I}\right] + E_2\left[\mathrm{II}\right] + E^{\mathrm{int}}\left[\mathrm{I},\mathrm{II}\right], \tag{A1}$$

where, $E_1[\mathrm{I}]$ and $E_2[\mathrm{II}]$ are the total energies in regions I and II with their respective calculation methods 1 and 2, and E^{int} is the interaction energy associated with coupling the two regions. We approximate this interaction energy by calculating each term using the EAM [52]:

$$E^{\mathrm{int}}\left[\mathrm{I},\mathrm{II}\right] = E_{\mathrm{EAM}}\left[\mathrm{I}+\mathrm{II}\right] - E_{\mathrm{EAM}}\left[\mathrm{I}\right] - E_{\mathrm{EAM}}\left[\mathrm{II}\right]. \tag{A2}$$

Substituting Eq. A1 into Eq. A2 and using KS-DFT as method 1 for region I and the EAM as method 2 for region II, the total energy can be written as

$$E\left[\mathbf{R^{tot}}\right] = E_{\mathrm{EAM}}\left[\mathbf{R}^{\mathrm{tot}}\right] - E_{\mathrm{EAM}}\left[\mathbf{R^{I}}\right] + \min_{\rho^{\mathrm{I}}} E_{\mathrm{DFT}}\left[\rho^{\mathrm{I}},\mathbf{R^{I}}\right], \tag{A3}$$

where $\mathbf{R}^{\mathrm{tot}}$, $\mathbf{R}^{\mathrm{I}}$ and $\mathbf{R}^{\mathrm{II}}$ are the coordinates in the respective regions and ρ^{I} is the electron density for the DFT calculation. Forces in region II are only based on the EAM. The coupling is due to the EAM forces across the EAM/DFT boundary; this is a direct result of approximating the interaction energy classically with the EAM. For atoms in region I that are farther away than r_c (the EAM cutoff radius) from the boundary separating the two

regions, the forces are based solely on DFT. For atoms that are within a distance r_c from the nearest region II atom, the net force is the sum of DFT contributions and the interaction correction $E_{\mathrm{EAM}}[\mathbf{R}^{\mathrm{tot}}] - E_{\mathrm{EAM}}[\mathbf{R}^{\mathrm{I}}]$. This involves DFT interactions with all region I atoms, and forces based on the EAM with atoms in region II that are within r_c. This approach is general and can be used for any type of system that requires quantum mechanical accuracy only in a small region of the total system.

We have chosen to employ QUICKSTEP (QS) [82] in our implementation of the multiscale code. This code, available in the suite of programs CP2K [55], is based on mixed Gaussian Plane Waves (GPW) [56]. The isolated center region I is non-periodic and typically this would require that a significant portion of the supercell consists of vacuum. This is computationally expensive and can lead to spurious results due to image effects if the size of the vacuum is not carefully converged. We circumvent this problem within the GPW formalism of CP2K by specialized Poisson solvers, which allow for fast convergence and accurate results, free of boundary effects [79–81]. The implementation is not limited to the 2D periodicity described in this work. An important point to highlight is that the impurity atoms in our implementation are treated by DFT only. Therefore, a classical EAM potential for the impurities is not required. This is a significant advantage, since constructing classical potentials that accurately describe the interaction between different types of atoms is exceedingly difficult and time-consuming.

Appendix B: Definition of decohesion and GBS mechanism terms

We will follow here the same labeling convention and definitions as in Ref. [3] and consider the following three processes: The 1) host removal (HR), 2) substitutional structure (SS) and 3) chemical and compressed impurity (CC) process for GB decohesion and GB sliding. A part of the total change in the GBS or decohesion energy can be assigned to each mechanism by considering the energy, $\gamma\,(x)$, of four different structures, $x = \mathrm{A}, \mathrm{B}, \mathrm{C}, \mathrm{D}$. Structures A and B are the fully relaxed structures of the pure Cu GB and the Cu GB with impurities, respectively. The energy difference between structures A and B simply gives the increase or decrease of the sliding or decohesion energy as impurities are added. To investigate the host removal process and its contribution to the overall change of the GBS or decohesion energy, we calculate structures D, which are based on the relaxed structures of the clean GB, that

is structure A, but with the Cu atoms that are replaced by substitutional impurities in B removed. The energy difference between structures A and D, $\Delta\gamma\,(\mathrm{HR}) = \gamma\,(\mathrm{D}) - \gamma\,(\mathrm{A})$, gives a measure of how much the loss of host bonds contributes to the overall energy change. Similarly, to address how significant the substitutional impurities change the structure of the surrounding host matrix, we calculate the difference between structures D and C, $\Delta\gamma\,(\mathrm{SS}) = \gamma\,(\mathrm{C}) - \gamma\,(\mathrm{D})$; the latter structure is based on structures B, but now with all impurity atoms removed. This gives a measure of how much the Cu matrix is distorted upon impurity addition, but without including the chemical effects of the impurities added by bonding in a different fashion than the Cu atoms. The host removal and substitutional structure processes, are purely mechanical processes. To capture the chemical interaction of the impurities we compare structures C and B, $\Delta\gamma\,(\mathrm{CC}) = \gamma\,(\mathrm{B}) - \gamma\,(\mathrm{C})$; this includes all the bonds introduced by the impurities.

---

[1] M. Yamaguchi, M. Shiga and H. Kaburaki, *Grain goundary decohesion by impurity segregation in a nickel-sulfur system*, Science 307 (2005), pp. 393-397.

[2] R. Schweinfest, A. T. Paxton and M. W. Finnis, *Bismuth embrittlement of copper is an atomic size effect*, Nature 432 (2004), pp. 1008-1011.

[3] A. Y. Lozovoi, A. T. Paxton and M. W. Finnis, *Structural and chemical embrittlement of grain boundaries by impurities: A general theory and first-principles calculations for copper*, Phys. Rev. B 74 (2006), pp. 155416-1 - 155416-13.

[4] J. R. Rice and J.-S. Wang, *Embrittlement of interfaces by solute segregation*, Mater. Sci. Eng. A 107 (1989), pp. 23-40.

[5] G. Schusteritsch and E. Kaxiras, *Sulfur-induced embrittlement of nickel: A first-principles study*, Modelling Simul. Mater. Sci. Eng. 20 (2012), pp. 065007-1 - 065007-15.

[6] A. P. Sutton and R. W. Balluffi, *Interfaces in Crystalline Materials*, Oxford University Press, Oxford, UK, 1995.

[7] F. R. N. Nabarro and H. L. de Villiers, *The Physics of Creep*, Taylor & Francis, London, 1995.

[8] P. Haasen, *Physical Metallurgy*, Cambridge University, Cambridge, UK, 1986.

[9] L. Lu, M. L. Sui and K. Lu, *Superplastic extensibility of nanocrystalline copper at room temperature*, Science 287 (2000), pp. 1463-1466.

[10] H. Van Swygenhoven and P. M. Derlet, *Grain-boundary sliding in nanocrystalline fcc metals*, Phys. Rev. B 64 (2001), pp. 224105-1 - 224105-9.

[11] D. Farkas, H. Van Swygenhoven and P. M. Derlet, *Intergranular fracture in nanocrystalline metals*, Phys. Rev. B 66 (2002), pp. 060101-1(R) - 060101-4(R).

[12] D. V. Bachurin and P. Gumbsch, *Accommodation processes during deformation of nanocrystalline palladium*, Acta Mater. 58 (2010), pp. 5491-5501.

[13] K. S. Kumar, H. Van Swygenhoven and S. Suresh, *Mechanical behavior of nanocrystalline metals and alloys*, Acta Mater. 51 (2003), pp. 5743-5774.

[14] J. Schiøtz, F. D. Di Tolla and K. W. Jacobsen, *Softening of nanocrystalline metals at very small grain sizes*, Nature 391 (1998), pp. 561-563.

[15] J. Schiøtz and K. W. Jacobsen, *A maximum in the strength of nanocrystalline copper*, Science, 301 (2003), pp. 1357-1359.

[16] J. Schiøtz, T. Vegge, F. D. Di Tolla and K. W. Jacobsen, *Atomic-scale simulations of the mechanical deformation of nanocrystalline metals*, Phys. Rev. B 60 (1999), pp. 11 971 - 11 983.

[17] N. Q. Vo, R. S. Averback, P. Bellon, S. Odunuga, and A. Caro, *Quantitative description of plastic deformation in nanocrystalline Cu: Dislocation glide versus grain boundary sliding*, Phys. Rev. B 77 (2008), pp. 134108-1 - 134108-9.

[18] L. Smith and D. Farkas, *Non-planar grain boundary structures in fcc metals and their role in nano-scale deformation mechanisms*, Philos. Mag., 94 (2014), pp. 152-173.

[19] E. O. Hall, *The deformation and ageing of mild steel: III Discussion of results*, Proc. Phys. Soc. B 64 (1951), pp. 747-753.

[20] N. J. Petch, *The cleavage strength of polycrystals*, J. Iron Steel Inst. London, 174 (1953), pp. 25-28.

[21] M. Dao, L. Lu, R. J. Asaro, J.T. M. De Hosson and E. Ma, *Toward a quantitative understanding of mechanical behavior of nanocrystalline metals*, Acta Mater., 55 (2007), pp. 4041-4065.

[22] K. Yang, H.-J. Fecht andY. Ivanisenko, *First direct in situ observation of grain boundary sliding in ultrafine grained noble metal*, Adv. Eng. Mater., 16 (2014), pp. 517-521.

[23] W. Hampe, *Beiträge zu der Metallurgie des Kupfers*, Zeitschrift für das Berg-, Hütten- und Salinenwesen in dem Preussischen Staate 22 (1874), pp. 93-138.

[24] W.R. Warke, *Liquid metal and solid metal induced embrittlement*, in *ASM Handbook Vol. 11*

Failure Analysis and Prevention, W. T. Becker and R. J. Shipley, eds., ASM International, Ohio, 2002, pp. 861-867.

[25] M.A. Tschopp, K.N. Solanki, F. Gao, X. Sun, M.A. Khaleel and M.F. Horstemeyer, *Probing grain boundary sink strength at the nanoscale: Energetics and length scales of vacancy and interstitial absorption by grain boundaries in α-Fe*, Phys. Rev. B 85 (2012), pp. 064108-1 - 064108-21.

[26] M. Rajagopalan, M.A. Tschopp and K.N. Solanki, *Grain boundary segregation of interstitial and substitutional impurity atoms in alpha-iron*, JOM 66 (2014) 129-138.

[27] N.R. Rhodes, M.A. Tschopp and K.N. Solanki, *Quantifying the energetics and length scales of carbon segregation to α-Fe symmetric tilt grain boundaries using atomistic simulations*, Model. Simul. Mater. Sci. Eng. 21 (2013), pp. 035009-1 - 035009-21.

[28] K.N. Solanki, M.A. Tschopp, M.A. Bhatia and N.R. Rhodes, *Atomistic investigation of the role of grain boundary structure on hydrogen segregation and embrittlement in α-Fe*, Metall. Mater. Trans. A. 44 (2013), pp. 1365-1375.

[29] M. Rajagopalan, M.A. Bhatia, M.A. Tschopp, D.J. Srolovitz and K.N. Solanki, *Atomic-scale analysis of liquid-gallium embrittlement of aluminum grain boundaries*, Acta Mater. 73 (2014), pp. 312-325.

[30] P.C. Millett, R.P. Selvam, S. Bansal and A. Saxena, *Atomistic simulation of grain boundary energetics: Effects of dopants*, Acta Mater. 53 (2005), pp. 3671-3678.

[31] D.E. Spearot, M.A. Tschopp, K.I. Jacob and D.L. McDowell, *Tensile strength of $\langle 100 \rangle$ and $\langle 110 \rangle$ tilt bicrystal copper interfaces*, Acta Mater. 55 (2007), pp. 705-714.

[32] S. Sanyal, Umesh V. Waghmare, P. R. Subramanian, and M. F. X. Gigliotti, *Effect of dopants on grain boundary decohesion of Ni: A first-principles study*, Appl. Phys. Letters 93 (2008), p. 223113-1 - 223113-3.

[33] G. Lu and N. Kioussis, *Interaction of vacancies with a grain boundary in aluminum: A first-principles study*, Phys. Rev. B 64 (2001), pp. 024101-1 - 024101-7.

[34] N. Du, Y. Qi, P. E. Krajewski, A. F. Bower, *Aluminum R3 grain boundary sliding enhanced by vacancy diffusion*, Acta Mater. 58 (2010), pp. 4245-4252.

[35] C. Molteni, N. Marzari, M. C. Payne and V. Heine, *Sliding Mechanisms in Aluminum Grain Boundaries*, Phys. Rev. Lett. 79 5 (1997), pp. 869-872.

[36] H.-B. Zhou, Y.-L. Liu, C. Duan, S. Jin, Y. Zhang, F. Gao, X. Shu and G.-H. Lu, *Effect of*

vacancy on the sliding of an iron grain boundary, J. Appl. Phys. 109 (2011), pp. 113512-1 - 113512-5.

[37] P. Ballo, J. Degmová and V. Slugeň, *Grain boundary sliding and migration in copper: Vacancy effect*, Phys. Rev. B 72 (2005), pp. 064118-1 - 064118-5.

[38] W.M. Yin a, S.H. Whang and R.A. Mirshams, *Effect of interstitials on tensile strength and creep in nanostructured Ni*, Acta Mater. 53 (2005), pp. 383-392.

[39] W.P. Green, M.A. Kulas, A. Niazi, K. Oishi, E.M. Taleff, P.E. Krajewski, and T.R. McNelley, *Deformation and failure of a superplastic AA5083 aluminum material with a Cu addition*, Metall. Mater. Trans. A, 37A (2006), pp. 2727-38.

[40] F. Weinberg, *Grain boundary shear in aluminum*, Trans. AIME, 212 (1958), pp. 808-17.

[41] M.D. Halliday and C.J. Beevers, *Some observations of grain-boundary sliding in aluminium bicrystals tested at constant strain rate and constant rate of stress increase*, J. Mater. Sci., 6 (1971), pp. 1254-1260.

[42] M. Kato, *Grain boundary sliding in high-purity aluminium bicrystal and Al-Cu solid solution bicrystal during plastic deformation*, Trans. Jpn. Inst. Met., 10 (1969), pp. 215-22.

[43] G. Mima, T. Oka, and T. Nishi, *On the grain boundary sliding of aluminum alloy bicrystals during the tensile test under constant stress and heating rate conditions*, J. Jpn. Inst. Met., 33 (1969), pp. 639-645.

[44] N. Du, . Qi, P. E. Krajewski, and A. F. Bower, *The effect of solute atoms on aluminum grain boundary sliding at elevated temperature*, Met. Mat. Trans. A, 2A, (2011), pp. 651-659.

[45] G. Duscher, M. F. Chisholm, U. Alber and M. Rühle, *Bismuth-induced embrittlement of copper grain boundaries*, Nature 3 (2004), pp. 621-626.

[46] A. Y. Lozovoi and A. T. Paxton, *Boron in copper: A perfect misfit in the bulk and cohesion enhancer at a grain boundary*, Phys. Rev. B 77 (2008), pp. 165413-1 - 165413-14.

[47] M. P. Seah, *Grain boundary segregation*, J. Phys. F 10 (1980), pp. 1043-1064.

[48] M. P. Seah, *Segregation and the Strength of Grain Boundaries*, Proc. R. Soc. Lond. A 349 (1976), pp. 535-554.

[49] J. R. Rice, *Dislocation nucleation from a crack tip: An analysis based on the Peierls concept*, J. Mech. Phys. Solids 40 (1992), pp. 239-271.

[50] R. O. Jones and O. Gunnarsson, *The density functional formalism, its applications and prospects*, Rev. Modern Phys. 61 (1989), pp. 689-746.

[51] S. M. Foiles, M. I. Baskes, and M. S. Daw, *Embedded-atom-method functions for the fcc metals Cu, Ag, Au, Ni, Pd, Pt, and their alloys*, Phys. Rev. B 33 (1986), pp. 7983-7991.

[52] N. Choly, G. Lu, W. E and E. Kaxiras, *Multiscale simulations in simple metals: A density-functional-based methodology*, Phys. Rev. B 71 (2005), pp. 094101-1 - 094101-16.

[53] X. Zhang and G. Lu, *Quantum mechanics/molecular mechanics methodology for metals based on orbital-free density functional theory*, Phys. Rev. B 76 (2007), pp. 245111-1 - 245111-10.

[54] X. Zhang, C.-Y. Wang and G. Lu, *Electronic structure analysis of self-consistent embedding theory for quantum/molecular mechanics simulations*, Phys. Rev. B 78 (2008), pp. 235119-1 - 235119-5.

[55] CP2K; software available at https://www.cp2k.org/.

[56] G. Lippert, J. Hutter and M. Parrinello, *A hybrid Gaussian and plane wave density functional scheme*, Mol. Phys. 92 (1997), pp. 477-487.

[57] J. P. Perdew, K. Burke and M. Ernzerhof, *Generalized gradient approximation made simple*, Phys. Rev. Lett. 77 (1996), pp. 3865-3868.

[58] S. Goedecker, M. Teter, and J. Hutter, *Separable dual-space Gaussian pseudopotentials*, Phys. Rev. B 54 (1996), pp. 1703-1710.

[59] M. Krack, *Pseudopotentials for H to Kr optimized for gradient-corrected exchange-correlation functionals*, Theor. Chem. Acc. 114 (2005), pp. 145-152.

[60] J. VandeVondele and J Hutter, *Gaussian basis sets for accurate calculations on molecular systems in gas and condensed phases*, J. Chem. Phys. 127 (2007), pp. 114105-1 - 114105-9.

[61] Y. Mishin, M. J. Mehl, D. A. Papaconstantopoulos, A. F. Voter and J. D. Kress, *Structural stability and lattice defects in copper: Ab initio, tight-binding, and embedded-atom calculations*, Phys. Rev. B 63 (2001), pp. 224106-1 - 224106-16.

[62] W. H. Press, S. A. Teukolsky, W. T. Vetterling and B. P. Flannery, *Numerical Recipes: The Art of Scientific Computing*, 3rd ed., Cambridge University Press, Cambridge, UK, 2007.

[63] J. Nocedal, *Updating quasi-Newton matrices with limited storage*, Math. Comp. 35 (1980), pp. 773-782.

[64] D.C. Liu and J. Nocedal, *On the limited memory method for large scale optimization*, Math. Prog. B 45, 3 (1989), pp. 503-528.

[65] E. D. Hondros and M. P. Seah, *"Segregation to interfaces*, Inter. Metals Rev. 222 (1977), pp. 262-301.

[66] T. Riedl, A. Kirchner, K. Eymann, A. Shariq, R. Schlesiger, G. Schmitz, M. Ruhnow and B. Kieback, *Elemental distribution, solute solubility and defect free volume in nanocrystalline restricted-equilibrium Cu-Ag alloys*, J. Phys.: Condens. Matter 25 (2013), pp. 115401-1 - 115401-9.

[67] P. M. Anderson and J. R. Rice, *Dislocation emission from cracks in crystals or along crystal interfaces*, Scr. Metall. 20 (1986), pp. 1467-1472.

[68] R. Thomson, *Crack stability and branching at interfaces*, Phys. Rev. B. 52, 19 (1995), pp. 14 245 - 14 253.

[69] J. R. Rice and R. Thomson, *Ductile versus brittle behavior of crystals*, Philos. Mag 29 (1974), pp. 73-97.

[70] U. V. Waghmare, E. Kaxiras, V. V. Bulatov and M. S. Duesbery, *Effects of alloying on the ductility of MoSi2 single crystals from first-principles calculations*, Modelling Simul. Mater. Sci. Eng. 6 (1998), pp. 493-506.

[71] U. V. Waghmare, E. Kaxiras and M. S. Duesbery, *Modeling brittle and ductile behavior of solids from first-principles calculations*, Phys. Stat. Sol. B 217 (2000), pp. 545-564.

[72] J. C. Slater, *Atomic radii in crystals*, J. Chem. Phys. 41 (1964), pp. 3199-3204.

[73] T. Surholt and C. Herzig, *Grain boundary self- and solute diffusion and segregation in general large angle grain boundaries in copper*, Def. Diff. Forum 1391 (1997), pp. 143-147.

[74] U. Alber, H. Müllejans and M. Rühle, *Bismuth segregation at copper grain boundaries*, Acta Mater. 47, 15 (1999), pp. 4047-4060.

[75] B. Zhou and E. A. Carter, *First principles local pseudopotential for silver: Towards orbital-free density-functional theory for transition metals*, J. Chem. Phys. 122 (2005), pp. 184108-1 - 184108-10.

[76] I. Shin, A. Ramasubramaniam, C. Huang, L. Hung and E. A. Carter, *Orbital-free density functional theory simulations of dislocations in aluminum*, Philos. Mag. 89 34 (2009), pp. 3195-3213.

[77] C. Huang and E. A. Carter, *Toward an orbital-free density functional theory of transition metals based on an electron density decomposition*, Phys. Rev. B 85 (2012), pp. 045126-1 - 045126-9.

[78] N. Choly and E. Kaxiras, *Kinetic energy density functionals for non-periodic systems*, Solid State Commun. 121 (2002), pp. 281-286.

[79] L. Genovesea, T. Deutsch and S. Goedecker, *Efficient and accurate three dimensional Poisson solver for surface problems*, J. Chem. Phys. 127 (2007), pp. 054704-1 - 054704-6.

[80] L. Genovesea, T. Deutsch, A. Neelov, S. Goedecker and G. Beylkin, *Efficient solution of Poisson's equation with free boundary conditions*, J. Chem. Phys. 125 (2006), pp. 074105-1 - 074105-5.

[81] P. E. Blöchl, *Electrostatic decoupling of periodic images of plane wave expanded densities and derived atomic point charges*, J. Chem. Phys. 103 (1995), pp. 7422-7428.

[82] J. VandeVondele, M. Krack, F. Mohamed, M. Parrinello, T. Chassaing and J. Hutter, *Quickstep: Fast and accurate density functional calculations using a mixed Gaussian and plane waves approach*, Comp. Phys. Comm. 167 (2005), pp. 103-128.